DICE

Report on work placement Applied Physics TU Delft, AP3911
Nikhef Amsterdam and Reactor Institute Delft
By Rudi Kalter
Student number: 1174096
Supervisor Nikhef: H. v.d. Graaf
Supervisor TU Delft: P. Dorenbos

Contents

Chapter 1

Introduction

In this report the DICE experiment is investigated. The main component, a time projection chamber (or TPC) is based on the drift chamber principle of determining the track position by measuring the time of drift of the primary electrons and determining the x and y coordinate on a pixel chip. With this, a reconstruction of the track in 3 dimensions is possible. The DICE experiment has a drift space of 20 mm and forms, with the TimePix pixelchip, a 'micro Time Projection Chamber' (μTPC).
With DICE it is possible to to measure cosmic ray events, but also events from radio active sources. This experiment is due to be installed in the RID nuclear reactor where short-living isotopes will be created to study Internal Pair Creation, a nuclear process in which a positron and electron are emitted simultaniously. With DICE we intend to measure the angular distribution of this process.

Chapter 2

Theory

2.1 Principles of Internal Pair Creation processes

Pair creation is a process in which an electron and a positron are simultaneously created in the electric field of an atomic nucleus. In pair creation processes, two types of pair creation are recognized: Internal and external pair creation. External pairs are created by high-energy gamma rays in the electric field of an atomic nucleus when a gamma ray passes through matter. Internal pairs are created directly in the de-excitation of excited nuclei. This is possible when the de-excitation energy exceeds the pair mass of 1.022 MeV/c^2. In this process energy and momentum must be conserved. In internal pair creation (IPC), the energies of the positron and the electron add up close to the transition energy minus the rest energy of the pair. The recoil of the nucleus will be small compared to the electron and positron energies. The angles between the positron and electron follow a distribution between 0 and 180 degrees which is characteristic for the nuclear transition [1] [2]. The distribution for an E2 transition, considered in section 2.2, is shown in figure 2.1.

2.2 Internal Pair Creation in ^{24}Mg

In this investigation IPC in ^{24}Mg is considered. Excited states of ^{24}Mg are produced in the beta decay process of ^{24}Na, which has a half life of 15 hours. In the decay of ^{24}Na, a 4+ state of ^{24}Mg is excited which decays with an E2

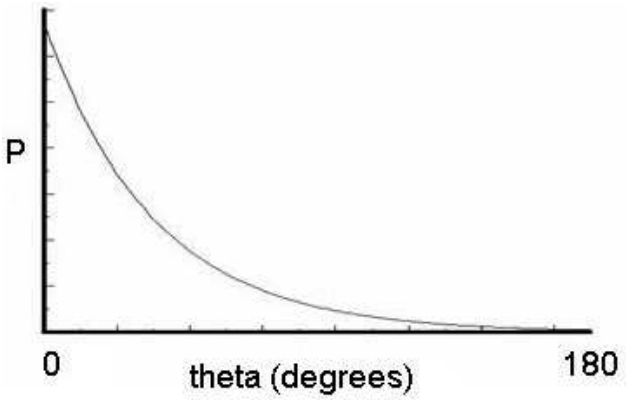

Figure 2.1: Distribution of angles between electrons and positrons from IPC in E2 transitions.

transition to the 2+ state. From this, the excited ^{24}Mg decays with an E2 transition to its ground state. In these E2 transitions, gamma's or electron-positron pairs are emitted simultaniously with the beta decay electrons. The decay scheme of ^{24}Mg from ^{24}Na is shown in figure 2.2.
The two transitions in ^{24}Mg with internal pair creation are 1368.675 KeV and 2754.028 KeV. For the 1359 keV transition internal pair creation occurs with a fraction of $(0.6 \pm 0.1) \times 10^{-4}$ of the total beta emission. And for the 2754 KeV transition internal pair creation occurs with a fraction of $(7.0 \pm 0.2) \times 10^{-4}$ of the total emission.

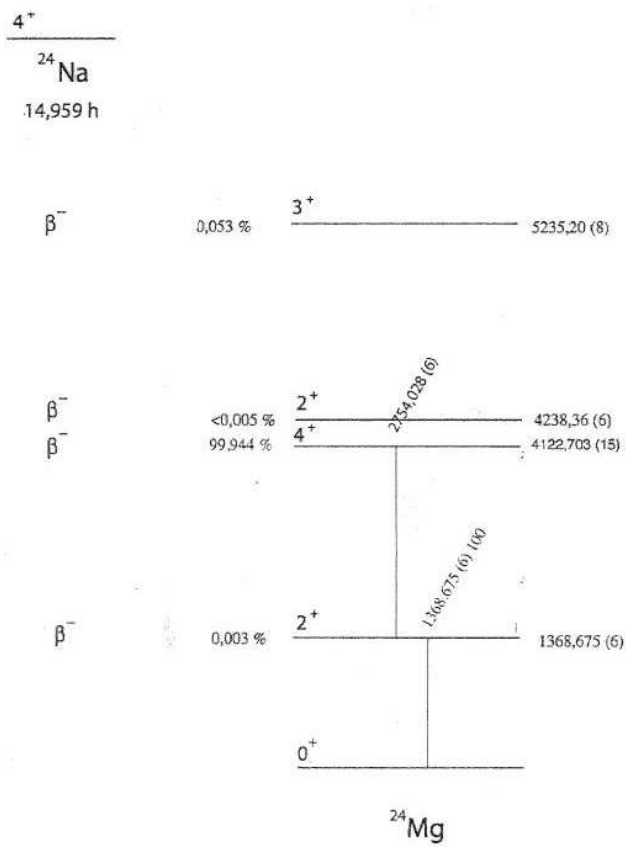

Figure 2.2: Decay scheme of ^{24}Na to exited states in ^{24}Mg.

2.3 Angular distribution of electron-positron pairs in E2 transitions

In IPC of different isotopes, anomalies in the predicted angular distribution are detected [1]. An explanation is that the anomalies are caused by the appearance of an X-boson, however, the existence of an X-boson hasn't been proven yet.
When the E2 transition of 2754 KeV occurs, an X-boson can be created with an energy $E_X = m_X + T_X$, where m_X is the mass of the X-boson and T_X is the kinetic energy of the X-boson. This X-boson decays very fast to an electron-positron pair, while the ^{24}Mg is in its 2+ state.
In the decay of the X-boson to an electron-positron pair, the pair will have a certain angular distribution. In the frame of reference of the X-boson, the electron and positron will allways travel in opposite directions. A certain

mass of the X-boson is assumed which suggests a certain kinetic energy, such that energy is conserved. Since the X-boson is moving, the positron and electron will travel with a certain angle with respect to each other in the lab frame of reference. This is visualized in figure 2.3.

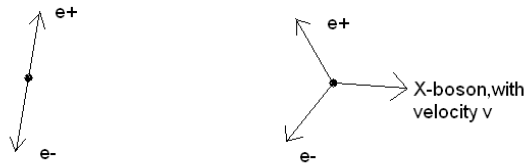

Figure 2.3: On the left the decay of an X-boson to an electron-positron pair is shown in the rest frame of the X-boson. On the right, the decay of a moving X-boson to an electron-positron pair is shown in the lab frame of reference.

Since IPC and the decay of the X-boson cannot be distinguished, the distributions of the correlation angles of the electron-positron pairs will add up. The distribution of the correlation angles of the electron-positron pairs formed from the decay of an X-boson is expected to be normal. When this normal distribution is added to the distribution given in figure 2.1, a small anomaly will be apparent. In figure 2.4 this anomaly is made visible. If the anomaly in the angular distribution can be proven, the existence of the X-boson would be indicated.

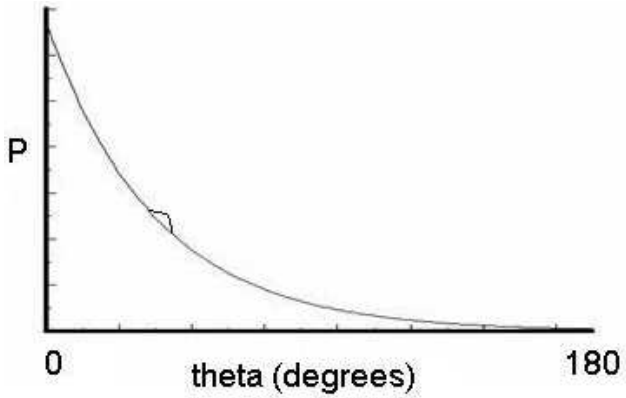

Figure 2.4: Anomaly in the distribution given in figure 2.1. The anomaly is very small compared to the overall distribution.

Chapter 3

Principles of working with DICE

3.1 Principles of DICE

The DICE chamber consists of a volume of $32.1 \times 32.1 \times 20$ mm^3, through which a gas mixture is flushed. On the bottom of the gas volume, a Gridpix chip (consisting of an Ingrid and a protection layer [11]) is placed to read out the signals. The chip is read out with a Muros device. A picture of the DICE chamber is shown in figure 3.1.

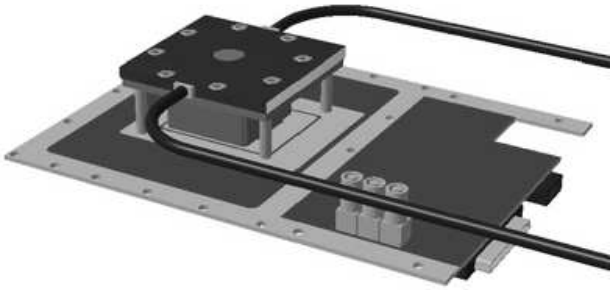

Figure 3.1: DICE setup. On the left the chamber is vissible, with cables coming to and from it for the injection and outflow of the gas. Below on the right the connector for the Muros data aquisitioning device is shown [7].

3.2 Electron multiplication in gas

When an energetic charged particle, like a muon, enters the drift volume it ionizes a molecule creating an electron-ion pair. Due to an applied electric field the electron drifts towards the pixel chip. It passes through a hole in the grid of the Timepix chip (section 3.3) where a large electric field is applied. In the strong electric field between the grid and the chip, each electron starts an avalanche. This is called electron multiplication and an extended study on this topic is given in the thesis by Maximilien Chefdeville [6]. When an avalanche has sufficient charge, it can be detected by a pixel.
A picture of a cross-section of the drift volume is given in figure 3.2 [9].

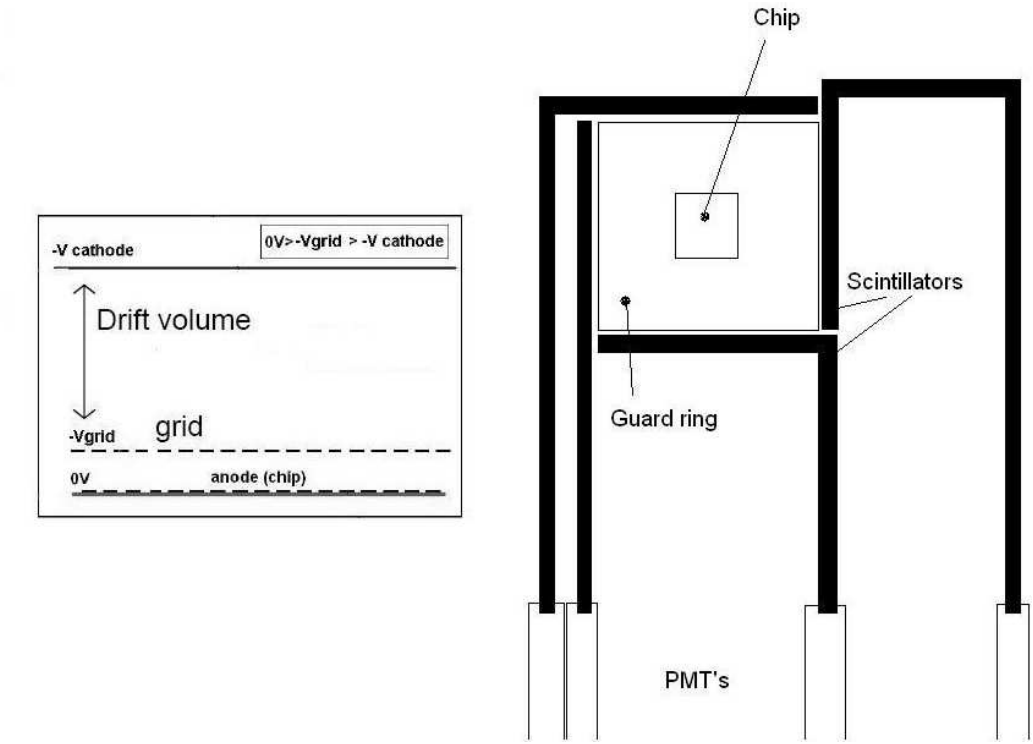

Figure 3.2: Left: Cross section of the TPC of the DICE experiment. The drift volume is 20 mm and the distance between the grid and the anode is 50 μm. The potential at the cathode is around -1050 V and the potential at the grid is around -400 V. On the right: Topview of the TPC, with scintillators around it. Around the grid a guard ring is placed at a potential slightly larger than the potential of the grid. This is done to create a homogeneous electric field.

3.3 Timepix chip

At the bottom of the DICE chamber a pixel chip is placed, which can collect charge on the pixel where an electron arrives. With the information from the pixel it is possible to determine the position of the electron and the time of drift. The chip is 16.12×14.11 mm^2 with 256×256 pixels, the size of the pixels is 55×55 μm^2. The chip is connected to a Muros interface which communicates with a computer equipped with the program Pixelman. Pixelman is explained in section 3.6.
For a linear response of the drift time with the drift distance, one wants the electric field around the chip to be homogeneous. For this purpose a guard electrode is placed around the chip (figure 3.2 and 3.3) parallel to the chip plane at a distance of 1 mm from the grid. This guard ring is placed at a potential, slightly larger than the potential of the grid. If this guard ring wasn't placed around the chip, the electric field lines would pile up at the edges of the chip, causing all the electrons to go to the edges.
Because there is a strong electric (avalanche) field between the grid and the chip, there is also a possibility that a discharge occurs. Such a discharge can damage a bare chip considarably. For this, chips are protected with a SiProt (Si_3N_4) layer.
Another point where damage may occur are the wirebonds of the chip. To protect the wirebonds as much as possible, a layer of silverglue is placed above it on the guard ring. This silverglue is connected to ground potential so that the electric field above the wirebonds is zero and no discharges occur in this region. A picture of this is shown in figure 3.3.

3.4 Triggering

When one measures radio active processes or cosmic ray events, a lot of unwanted events can be recorded, this should be prevented. For this purpose a trigger system is installed. For cosmic ray events, the DICE chamber is placed such that the cathode and the anode are vertical. Four scintillators are placed such that the drift volume is sandwiched between them, this is shown in figure 3.2. When a charged particle, like a muon, crosses a scintillator there will be a pulse in the form of a small flash of light. This lightpulse propagates to a photo multiplier tube (PMT) which converts the lightpulse to a fast electric signal. This electric signal is sent to electronics containing an and-gate. When a particle crosses both scintillators at the same time, a coincedence is recorded in the electronic device.
A muon with cosmic origin usually goes straight through the gas volume, so

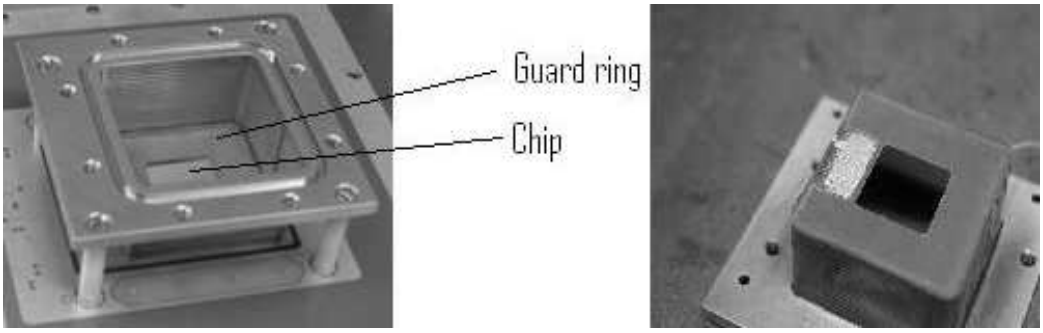

Figure 3.3: Left: DICE chamber, opened up so the guard ring and the chip are vissible. On the right: The DICE chamber upside down and detached from the ground plate. The shiny part in the centre of the picture is the silverglue. This is connected to the ground potential and is placed on the guard ring above the wirebonds to prevent discharges.

when there is a pulse on the upper and lower scintillator, a coincedence is recorded and a trigger is set to initiate a recording.
For IPC events a sample of ^{24}Na is placed inside the gas volume. Since there are three particles per IPC event, a three hit trigger is needed. A picture of the DICE with 4 scintillators is shown in figure 3.4.
The volume of the DICE chamber is larger than the drift volume of the chip. This means that it is possible that a trigger is set, while no signal is recorded. It is also possible that a coincedence occurs from other events. This kind of errors influence the effectiveness of the triggersystem.

3.5 Charged particles in a magnetic field

As shown in figure 3.4 the drift volume of the DICE chamber is placed between two magnets. The magnetic fields produced by these magnets is rather homogeneous and parallel to the electric field. The magnetic field produced by these magnets is approximately 0.12 T.
When a charged particle crosses a magnetic field it experiences a Lorentz force, given by:

$$\overrightarrow{F} = q \cdot (\overrightarrow{E} + \overrightarrow{v} \times \overrightarrow{B}) \tag{3.1}$$

Where q is the charge of the particle, $\overrightarrow{v}$is the velocity of the particle and $\overrightarrow{B}$ is the magnetic field. Since the electrons drift along the electric field, they

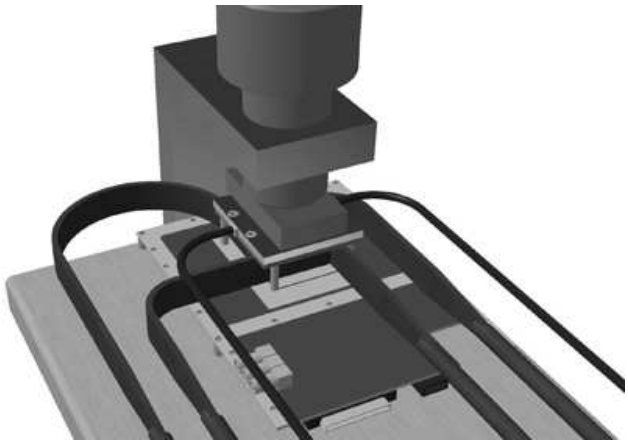

Figure 3.4: Here we see the DICE chamber with 4 scintillators placed around it, the ends of the scintillators go to the PMT's. In this picture DICE is also placed between 2 magnets, due to these magnets it is possible to collect data on the energies of detected particles [7].

also drift along the magnetic field and no Lorentz force is exerted on these electrons by the magnetic field. The particles that do experience a Lorentz force from the magnetic field are charged particles that travel in a direction with a perpendicular component to the magnetic field.
A cosmic muon can cross the scintillators, moving perpendicular to the magnetic field. According to equation 3.1 the track of the muon will be bent. It is also possible that an anti-muon crosses the magnetic field, this track will be bent the other way.
From the way in which the track of a charged particle is bent, the momentum of the particle can be estimated. The momentum is proportional to the curvature of the track.

3.6 Pixelman

Pixelman is a program, developed to read out the data from the Timepix chip. With Pixelman it is possible to set a threshold for a pixel to detect a charge signal. When a new chip is connected, one can perform a threshold equalization. When this is done, the pixels on the chip all have the same threshold to a charge signal. After that one can set the amount of charge-signal which is desired, so pixels only give a signal when they are actually hit and no noise is recorded.

The chip can be used in different modes.
First the time-over-threshold (ToT) mode: the registered number of counts is equal to the number of clock cycles elapsed during the time the pulse was above the threshold. This time, and thus the number of counts, is a rising function of the input charge signal.
Another possibility is the time mode: the number of counts is equal to the number of clock cycles counted during the time between the pixel hit and the end of the shutter time. This time is shorter for hits recorded at the end of the shutter time than hits recorded at the beginning, from this the drift time can be extracted [6].
Most of the aquisitions are done in the time mode, with which it is possible to reconstruct tracks in three dimensions.

Chapter 4

Data analysis

4.1 The Hough transform

The Hough transform is used to detect the presence of patterns and shapes in images, such as straight lines, ellipses and circles.[1]

Straight lines

The first case of a Hough transform is a straight line, represented by $y = a \cdot x + b$. This relation for a straight line can be represented by a point (a, b) in the parameter space. For computational reasons we parameterize the lines in the Hough transform with two other parameters, r and θ. Here r represents the distance from the line to the origin and θ represents the angle from the origin to its closest point. This is made vissible in figure 4.1. When we use this parametrization, the equation for the straight line becomes:

$$y = \left(-\frac{\cos(\theta)}{\sin(\theta)}\right) \cdot x + \frac{r}{\sin(\theta)} \tag{4.1}$$

Which can be rearranged to

$$r = x \cdot \cos(\theta) + y \cdot \sin(\theta) \tag{4.2}$$

If $\theta \in [0, \pi]$ and $r \in \Re$ each line can be associated to a point (r, θ), where the (r, θ) plane is referred to as the Hough space.

[1] Initially the Hough transform was used for image detection in bubble chamber photographs by Hough in 1959. In 1962 the Hough transform was patented and assigned to the U.S. Atomic Energy Commission with the name "Method and Means for Recognizing Complex Patterns". The method used today was first described in 1972 [13].

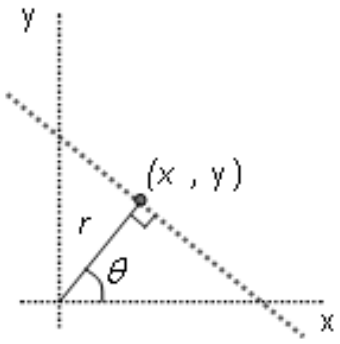

Figure 4.1: Coordinates r and θ as used in the Hough transform, equation 4.1.

For every point x_0 and y_0 an infinite number of lines can pass through it and all the lines that do obey the equation:

$$r(\theta) = x_0 \cdot \cos(\theta) + y_0 \cdot \sin(\theta) \tag{4.3}$$

This corresponds to sinusoidal curves in the Hough space. Now a set of points that form a straight line will produce sinusoidals which cross through the same point. A sample is given in figure 4.2 and. From this, one only needs to detect the r and θ to implement it in equation 4.1.

Circles

As mentioned, the Hough transform can also be used to detect circles and ellipses.
For a circle we have the following equation:

$$R^2 = (x - x_0)^2 + (y - y_0)^2 \tag{4.4}$$

When we use a fixed value of R, we are left with 2 unknowns, x and y. These unknowns can be parameterized by a standard parameterization of the circle:

$$\begin{aligned} x &= R \cdot \cos(\theta) + x_0 \\ y &= R \cdot \sin(\theta) + y_0 \end{aligned} \tag{4.5}$$

And as can be seen: $(x - x_0)^2 + (y - y_0)^2 = R^2$.
If there is a set of datapoints, every datapoint can be used as the centre of infinitely many circles. In figure 4.3 a set of datapoints is shown with Hough

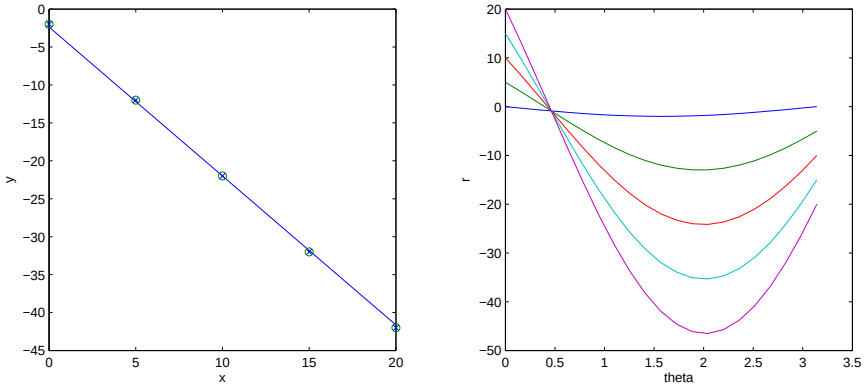

Figure 4.2: On the left, points are laying on a straight line. Different lines are drawn through a point and the distance r from this line to the origin is calculated. For different values of r we get different values of θ. On the right the Hough space is drawn and we see that all the lines go through one point (r, θ). This r and θ are the parameters in equation 4.1 and parameterize the straight line.

transforms of different radiï. It can be seen that a search for the right value of R is needed to create the best fit. The best R is the one which has the highest density in the neighbourhoud of the cross section of the circles. In figure 4.3 this is $R = 5$ obviously.

Multiple tracks

In trackfinding, it is possible that two tracks appear in the same graph. In such a graph only the track with the highest density in its Hough transform will appear if one makes a fit of the tracks. This is different from a polynomial fit, which takes some sort of avarage of the two tracks. What two straight tracks look like in the Hough space can be seen in figure 4.4. The Hough transform now only fits the track with the highest density at the intersection in the Hough space. To be able to make two fits in this case, we need to isolate the two points with a local maximum. To do this, the points involved with the highest density will be used to fit a line. Then they are separated from the other datapoints. On the reduced set of datapoints, again a Hough transform is performed and a second line can be fit.

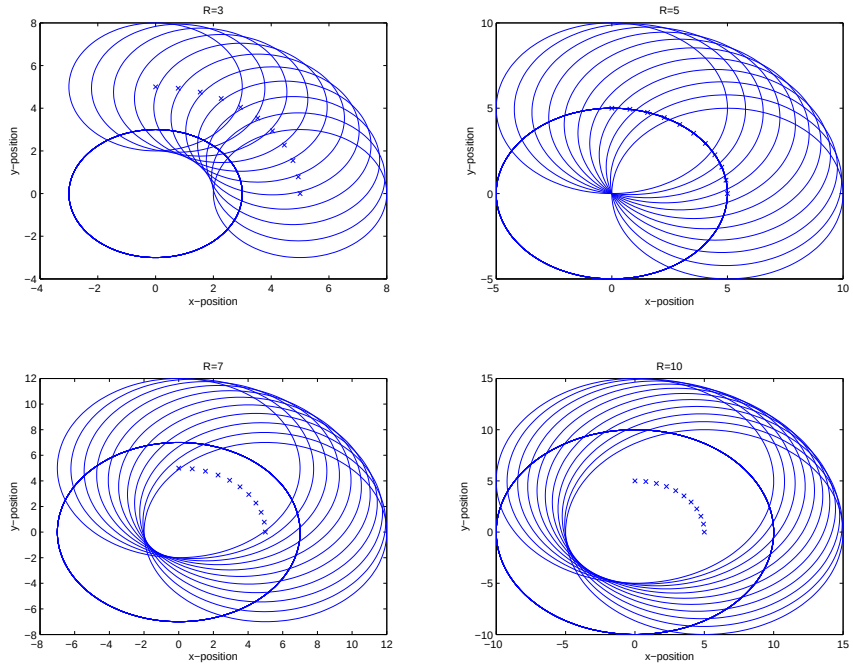

Figure 4.3: A set of data is generated. The datapoints lie on a circular trajectory and circles around the datapoints are created with different radiï. It can be seen that for $R = 5$ the transform gives the best fit.

4.2 Fitting with a polynomial

From the above it can be seen that the Hough transform is particularly useful for separating different tracks in a dataset.
Once the tracks are separated, an accurate track fit can be performed. For this a least squares analysis with a polynomial is used. A polynomial is a function of the form:

$$y = a_n \cdot x^n + a_{n-1} \cdot x^{n-1} + ... + a_1 \cdot x + a_0 \tag{4.6}$$

Results of fitting tracks with a polynomial will be given in chapter 5.

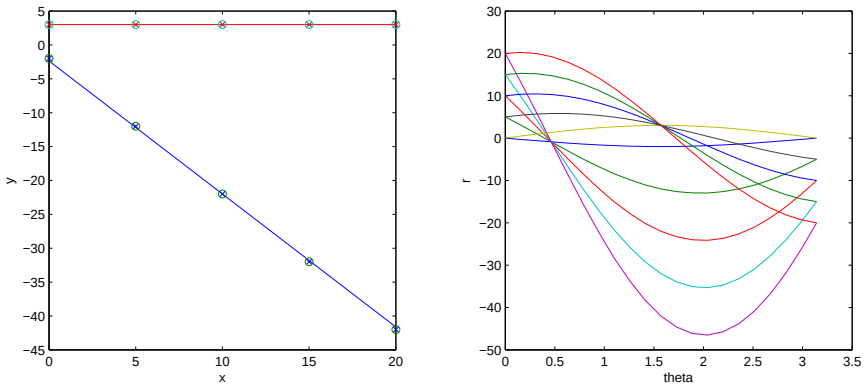

Figure 4.4: On the left, two straight lines are displayed. On the right the Hough transform is shown. We see that there are two points where a lot of the tracks pass through.

Chapter 5

Results

5.1 Tracks from cosmic ray events

The DICE chamber has been equipped with a triggering system for cosmic ray events. The scintillators have a surface of approximately 3×1.7 cm^2, they are shown in figure 3.4. Through this surface a cosmic muon crosses about once a minute. In Pixelman a filter is set, which makes sure that a minimum number of pixels is hit before a track is actually recorded. In figure 5.1 the recording of a cosmic ray event is shown. The track is roughly straight although around the DICE chamber strong magnets are placed. This shows that the cosmic muons have a high momentum.
Since we assume highly energetic particles with a straight track, we can use a polynomial of order one. The result for a cosmic ray event is given in figure 5.2.

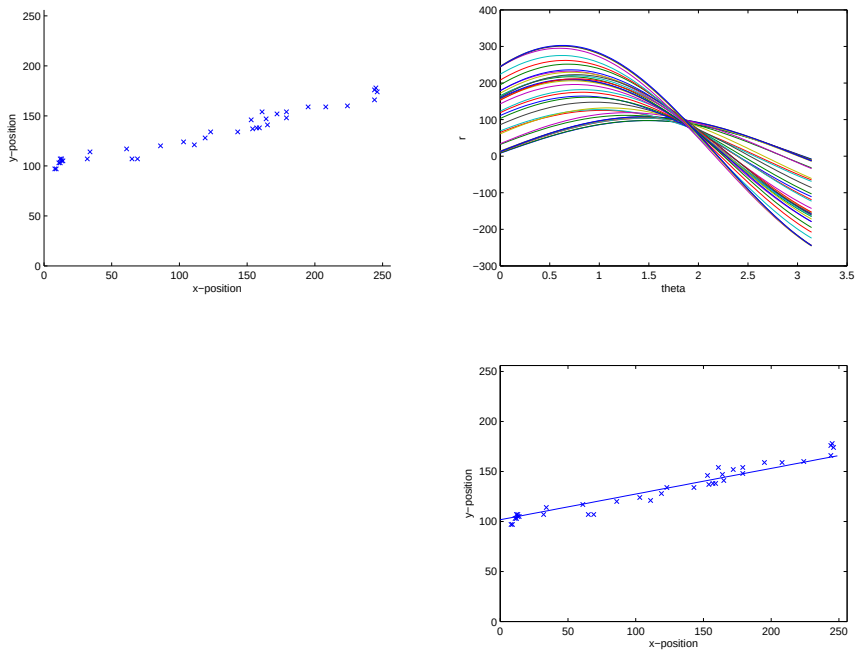

Figure 5.1: Result for a muon, originating from a cosmic shower. In the upper left we see the data from the chip. The upper right graph shows the Hough transform of the track, a maximum density is around $r = 100$ and $\theta = 1.75$. Below on the right the resulting fit of the Hough transform is shown.

5.2 ^{90}Sr tracks

5.2.1 Single track

With DICE a measurement of curved tracks from a ^{90}Sr source is performed. For this purpose, no trigger system was used. In Pixelman the aquisition time was lowered such that most recordings have only one track. Again a minimum number of hit pixels is required to save a track.
A recording of a ^{90}Sr track is shown in figure 5.3. The track is curved, due to the magnets placed around the DICE chamber. From this it can be concluded that the ^{90}Sr tracks have a smaller momentum than the tracks from the cosmic muons, since they are much more affected by the magnetic field. The result for a polynomial of order three is shown in figure 5.4.

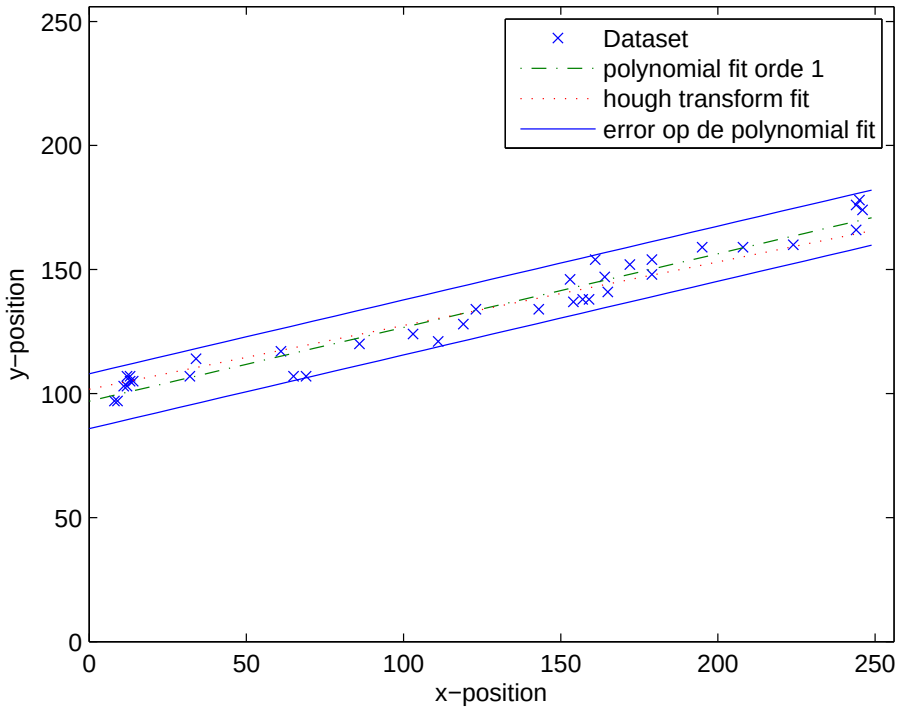

Figure 5.2: Fit of the track of a cosmic muon with a polynomial of order one and with the Hough transform. The outer band show the confidence interval of the polynomial.

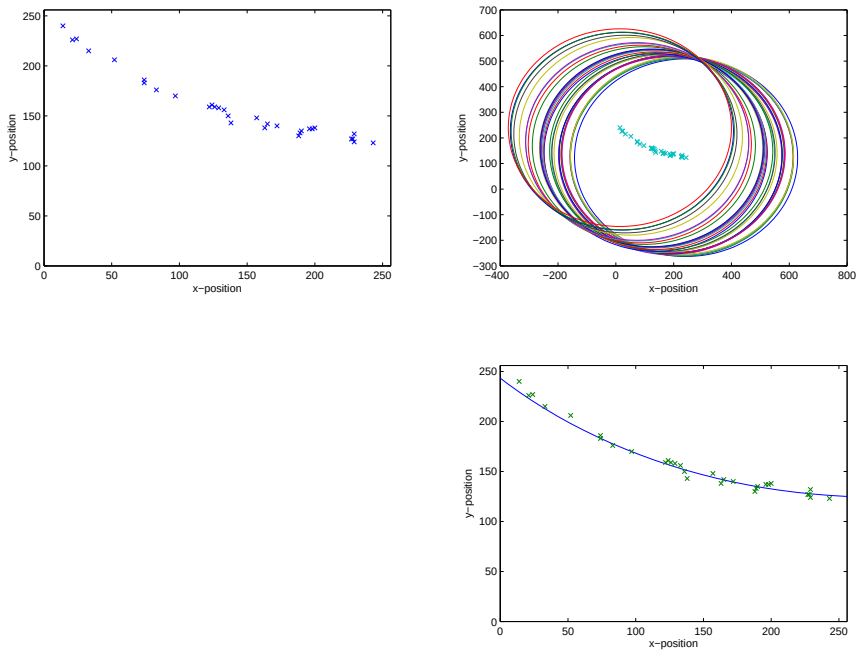

Figure 5.3: Result for an ^{90}Sr event. In the upper left we see the data from the detector. The upper right graph shows the Hough transform of the track, the maximum density is around $x_0 = 250$ and $y_0 = 500$. R is detected by testing several values of R and detecting the maximum density. With these values we can fill in the parametrization, equation 4.6, for the circle that fits the datapoints the best. Below on the right the resulting fit of the Hough transform is shown.

5.2.2 Multiple tracks

In ^{90}Sr track finding it is possible to find more than one track in one fit. Now the filtering strength of the Hough transform is demonstrated in figure 5.5. First the Hough transform is used to separate the two tracks from the dataset, then a polynomial of order three is used to make an accurate fit. With this polynomial, the result of figure 5.5 becomes as shown in figure 5.6.

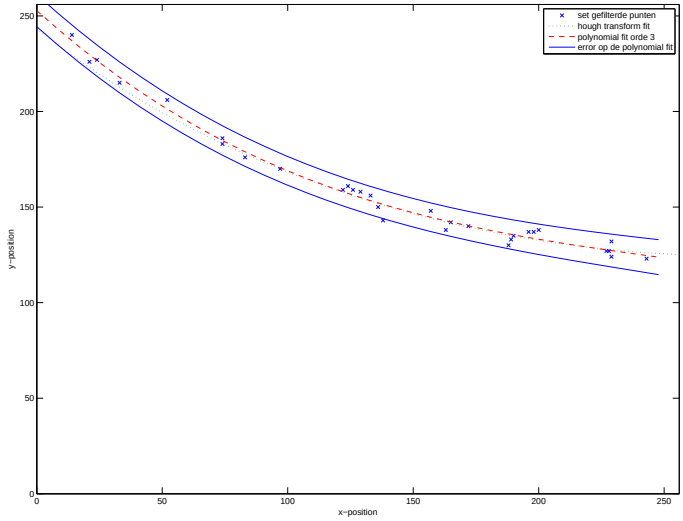

Figure 5.4: Fit of the track of a beta particle from an Sr^{90} source with a polynomial of order three and with the Hough transform. The outer band show the confidence interval of the polynomial.

5.3 IPC events

In the search for IPC events, a radio active source of ^{24}Na was prepared at the Reactor Institute Delft. This ^{24}Na source was placed inside the drift volume. In the first few days this source was very active, so a selective trigger system was nescessary. At this point only a triggersystem with two scintillators was available. The scintillators were situated perpendicular to each other to collect data from IPC events in one corner of the DICE chamber. Unfortunately this trigger was not very effective, so from the recordings IPC events had to be filtered on sight. A possible IPC event is shown in figure 5.7. In the figure, 3 tracks originate at a starting point, two of the tracks have a curvature in the same direction and one has an opposite curvature. This shows that this is a possible IPC event, because in a magnetic field a positron has an opposite curvature from an electron.

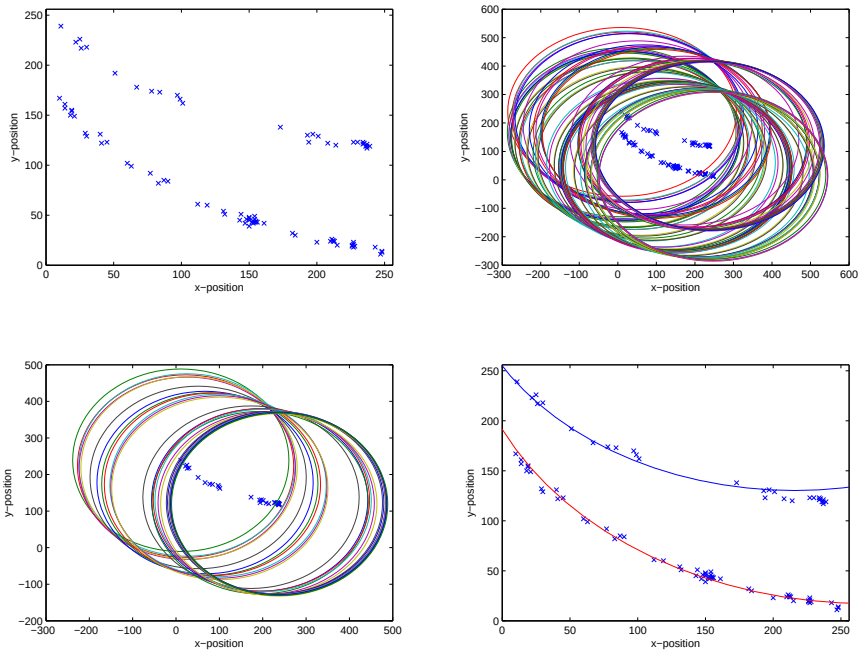

Figure 5.5: Result for a double ^{90}Sr event. In the upper left we see the result from the chip. The upper right graph shows the Hough transform of the tracks. There are two local maxima, around $(x_0, y_0) = (250, 300)$ and one around$(x_0, y_0) = (250, 450)$. First the track with the highest density is drawn and the points that weren't used are filtered. Then the points that are filtered are transformed to the Hough space again, shown on the lower left. The resulting two fits are shown in the figure in the lower right.

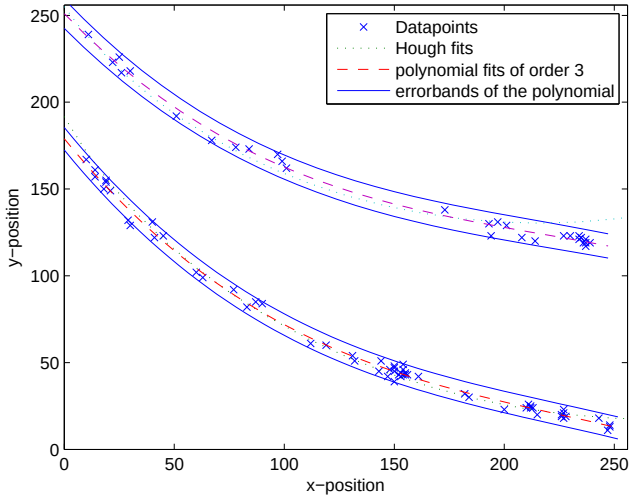

Figure 5.6: ^{90}Sr double track fit with a polynomial of order three and with the Hough transform. The outer bands show the confidence interval of the polynomial.

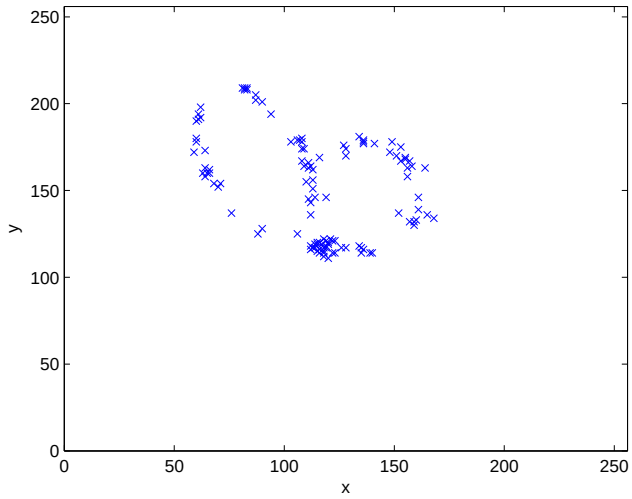

Figure 5.7: Example of an IPC event. The tracks originate approximately at$(x, y) = (130, 120)$.

Chapter 6

Conclusions

In this report, results of working with the DICE detector are presented. It is shown that DICE can collect position data of charged particles. For collecting these data with position information a 2 coincidence trigger system was developed which works. This triggersystem can be expanded to a 3 or 4 coincedence triggersystem.

For the data analysis a study on the Hough transform was done. My conclusion is that the Hough transform is particularly useful for the separation of different tracks in one dataset. With the Hough transform we did not get accurate fits with an error estimation. For this, when the different tracks in a dataset are separated, a least squares method should be used to make an accurate fit. Further work on this topic includes 3D tracks and fits.

In processing IPC events, the Hough transform hasn't proven itself to work just yet. Since the tracks of the three charged particles can be very close together, the Hough transform has difficulties separating the different tracks. When this separation can be done properly, it can be possible to fit 3D tracks through the different tracks in the datasets. With these tracks it should be possible to analyze data on the angular distribution of the electron-positron pairs produced in the IPC events.

Bibliography

[1] De Boer, F., Anomalous Internal Pair Conversion Signaling Elusive Light Neutral Particles, Nikhef, November 4, 2005.

[2] M.E. Rose, Phys. Rev. 76 (1949) 678, see also Phys. Rev. 78 (1950) 184 (Erratum); Phys. Rev. 131 (1963) 1260.

[3] Huang,K., Internal pair creation in beta decay. Physical review, volume 102, number 2, April 15, 1956.

[4] Horton, G.K., Angular distribution in internal pair creation, 1947.

[5] Alburger, D.E., Beta Decay of N^{16}. Physical review, volume 111, number 6, September 15, 1958.

[6] Chefdeville, Maximilien Alexandre. Development of Micromegas-like gaseous detectors using a pixel readout chip as collecting anode. 15 Jan. 2009, Nikhef Phd Thesis.

[7] http://www.nikhef.nl/pub/departments/mt/projects/detectorR_D/, April 2009.

[8] v.d. Graaf, H. et. al., Recent GridPix results: An integrated Micromegas grid and an ageing test of a Micromegas chamber. Nucl. Instr. and Meth. A 566 (2006) 62-65.

[9] Bilevych, Y. et.al. Gridpix, the digital bubble chamber. Nikhef and University of Twente.

[10] Colas, P. et. al.,The readout of a GEM or Micromegas-equipped TPC by means of the Medipix2 CMOS sensor as direct anode. Nucl. Instr. and Meth. A 535 (2004) 506.

[11] Campbell, M. et. al., An integrated readout system for drift chambers: the application of monolithic CMOS pixel sensors as segmented direct anode. Nuclear Physics B (Proc. Suppl.) 150 (2006) 200-203.

[12] Campbell, M. et. al.,GOSSIP: A vertex detector combining a thin gas layer as signal generator with a CMOS readout pixel array. Nucl. Instr. and Meth. A 560 (2006) 131-134.

[13] Duda, R. O. and P. E. Hart, Use of the Hough Transformation to Detect Lines and Curves in Pictures, Comm. ACM, Vol. 15, pp. 1115 (January, 1972).

[14] Ujaldon, M. et. al., On the computation of the circle Hough transform by a GPU rasterizer. Pattern Recognition Letters 29 (2008) 309-318.

[15] Ioannou, D. et. al., Circle recognition through a 2D Hough transform and radius histogramming. Image and Vision Computing 17 (1999) 15-26.